ADVANCED
FUNCTIONAL
MATERIALS
www.afm-journal.de

Materials Views
www.MaterialsViews.com

Self-Assembled Platinum Nanochain Networks Driven by Induced Magnetic Dipoles

*Min-Rui Gao, Shi-Ran Zhang, Yun-Fei Xu, Ya-Rong Zheng, Jun Jiang, and Shu-Hong Yu**

Developing a reliable technique to organize nanoscale building blocks into ordered one-dimensional assemblies is of particular interest in a range of practical applications. Here, for the first time, it is reported that platinum (Pt) nanoparticle chain networks can be assembled spontaneously in solution on a large scale. The in-situ induced magnetic dipoles are believed to be the driving force for producing such elegant assembled nanochains. The alterant electronic structure of Pt modified by a very thin layer of polyvinylpyrrolidone (PVP) molecules leads to the ferromagnetism of Pt (a traditional paramagnetic metal), which has been verified by a series of analysis techniques and theoretical modeling. The temperature- and time-dependent nucleation, growth, and organization processes of Pt chain networks are carefully investigated. These findings not only present the uncommon ferromagnetism of Pt, but also raise a possibility for expanding this strategy towards other assemblies of nonmagnetic nanoscale building blocks.

1. Introduction

One-dimensional self-assembled nanostructures are of particular interest in nanoelectronics, optoelectronics, nanomagnetism, and biosensing devices,[1] which were often formed from ferromagnetic and superparamagnetic nanoparticles on supporting surfaces[2–5] or in solutions.[6] Nanoparticle chains are much less known for nonmagnetic materials although they can form for nonmagnetic semiconductors and metals, due to the complex interparticle interactions involving electrostatic interactions and other forces.[1,7–10] Finding their new examples and interactions that could contribute to their formation would be potentially useful.

Recent discovery of ferromagnetism in Pt nanoscale systems has generated great attention for basic investigations as well as for practical applications, for example, in data storage.[11–15] It is well known that Pt bulk metal is paramagnetic, in which the magnetic anisotropy (that is, the intrinsic preference of magnetization to lie along an easy axis) is very small due to the orbital momentum of the electrons is strongly quenched by crystal fields.[13] However, on the nanometer scale, more Pt atoms will be located at the surface of the nanocrystal, leading to the resurrection of the orbital moment at lower coordinated surfaces and thus a larger magnetic anisotropy energy. Similar phenomenon was also suggested in other 4d and 5d noble metals and alloys such as Pd, Au, and Au/Pt in the nanodimension, whereas their bulk counterparts are nonmagnetism.[16–21] In these confined nanostructures, narrower electron bands induced by the reduced coordination number of surface atoms yield a larger density of states n(E_F) at the Fermi level and thus more easily satisfies the Stoner criterion for ferromagnetiam n(E_F)$\cdot J > 1$, where J is exchange integral.[22]

Besides the size effects, the origin of ferromagnetism in nanocrystals was also attributed to the change in electronic structure. For examples, the change in electronic structure of Au nanoparticles and thin films has been recently found after capping them with organic molecules and accordingly induces their ferromagnetic behavior, although bulk Au is diamagnetic.[20,23,24] When thiols are chemisorbed on Au surface, the charge can transfer from the Au to the S, leading to the increase of 5d density of holes at the Au site. As a result, a localized magnetic moment fixed along the bond direction was formed, enabling ferromagnetism even at room temperature (RT).[20] Except the noble metal nanosystems, similar observations have also been discovered in organically coated semiconductors such as ZnO,[25,26] ZnS,[27] CdSe,[28] and PbS.[29] Recently, Sakamoto et al. proclaimed another mechanism for ferromagnetism based on their theoretical and experimental studies.[15] In that case, a decrease in the 5d hole number was found through the *s–d* rehybridization and lead to a stronger modification of electronic structure in a nanodiamensional system.[30]

Herein, we report for the first time that Pt nanoparticle nanochain networks can be directly assembled in solution due to induced magnetic dipoles originated from the alterant electronic structure modified by the capped polyvinylpyrrolidone (PVP) molecules. Our results presented here not only support the observation of ferromagnetism in traditional nonmagnetic

---

Dr. M.-R. Gao, S.-R. Zhang, Y.-F. Xu, Y.-R. Zheng,
Dr. J. Jiang, Prof. S. H. Yu
Division of Nanomaterials and Chemistry
Hefei National Laboratory for
Physical Sciences at Microscale
Department of Chemistry
University of Science and Technology of China
Hefei, Anhui, 230026, P. R. China
E-mail: shyu@ustc.edu.cn

DOI: 10.1002/adfm.201302262

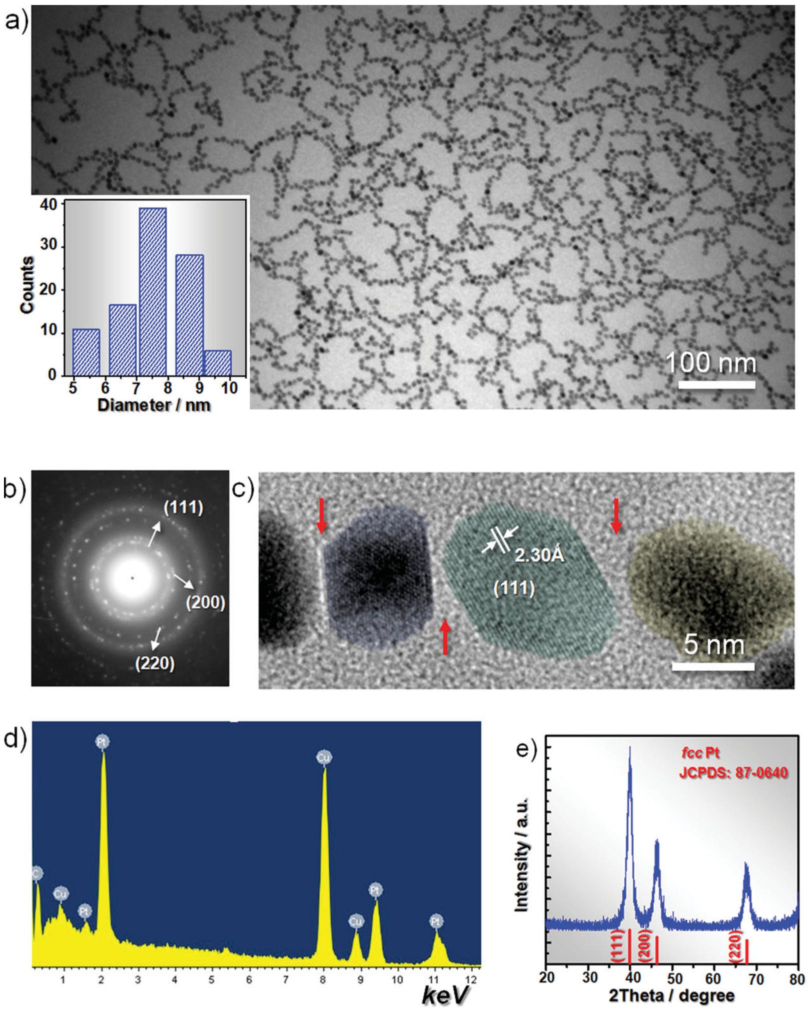

Figure 1. a) TEM image of Pt nanoparticle chain networks synthesized at 160 °C for 18 h. Inset shows the corresponding particle-size histogram. b) The SAED pattern taken from the top right corner in (a). c) HRTEM image of a typical Pt nanoparticle chain. d,e) EDS spectrum and XRD pattern of the Pt nanoparticle chain networks, respectively.

Pt but also suggest the possibility of using such magnetism as an intrinsic driving force to construct other assembled structures of nonmagnetic nanoscale building blocks.

2. Results and Discussion

2.1. Characterization of Pt Chain Networks

Transmission electron microscopy (TEM) image in **Figure 1**a shows that the overall morphology of the sample is composed of network-like structures. The individual Pt chain including closed loops and branched superstructures often extends to hundreds of nanometers in length and consists of tens of nanoparticles with an average size of about 7.6 nm (Inset in Figure 1a). The corresponding selected-area electron diffraction (SAED) pattern shown in Figure 1b highlights not only continuous rings indexed to (111), (200), (220) planes of Pt, but also discrete diffraction spots that comes from the substructure of the whole ensemble of nanoparticles. Figure 1c shows the high-resolution TEM (HRTEM) image of several assembled nanoparticles extracted from a typical Pt chain, from which a lattice spacing of 2.30 Å can be observed, corresponding to the (111) facet of face-centered cubic (fcc) Pt. It should be noticed that interparticle gap (≈0.7 nm) between adjacent Pt nanoparticles can be clearly seen (marked by red arrows), which is quite different from previously reported Au chains governed by electric dipoles,[1,10] for which the adjacent nanoparticles were often in close contact within the chains. Although the presence of PVP can be detected by Fourier transform infrared (FTIR) spectrum discussed below, the polymer coating is almost invisible in Figure 1c, indicating that PVP molecules form a very thin layer on the surface of the Pt nanoparticles. The composition and crystal phase purity of the product were analyzed by energy dispersive X-ray spectrometry (EDS) and powder X-ray diffraction (XRD) techniques, respectively (Figures 1d,e). As expected, the EDS spectrum only reveals Pt signal from the Pt nanochain networks, where Cu and C peaks emanate from the carbon-coated TEM grid (Figure 1d). The XRD pattern (Figure 1e) shows that all of the reflections can be indexed to fcc Pt with a lattice constant $a = 0.391$ nm (JCPDS Card no. 87–0640).

2.2. Effect of Temperature on the Pt Nanostructures

It was found that the morphology and self-assembly behavior of the Pt nanoparticles are very sensitive to the change of reaction temperature (**Figure 2**). When the reaction vessel was heated at 90 °C for 18 h, small nanoparticles (≈3.1 nm) with high dispersibility were obtained (Figures 2a,a'). Reaction at 110 °C yielded uniform Pt nanostars (Figures 2b,b'). This star-like nanostructure was frequently observed in the homogeneous nucleation and then overgrowth of Pt, for which low concentration of seeds and high concentration of Pt atoms were necessary.[31,32] In our system, the ideal temperature for sustaining the prerequisite of the overgrowth mechanism and leading to the formation of Pt nanostars is 110 °C. The reaction at 130 °C also yielded star-like Pt (Figures 2c,c'). Noticeably, some self-assemblies of star-like nanoparticles began to appear (marked by red arrows). When switching the temperature to 150 °C, relatively uniform Pt chain networks were obtained (Figures 2d,d'). Here, two points are worth highlighting: one is that the length of chains is much shorter than that prepared at 160 °C (Figure 1a); the other is that the building units of Pt chains are not nanostars but spherical nanoparticles. Such morphology change could be attributed to higher temperature applied: the decomposition of Pt precursor and subsequent particle growth occurred at a very fast reaction rate at 150 °C, so the

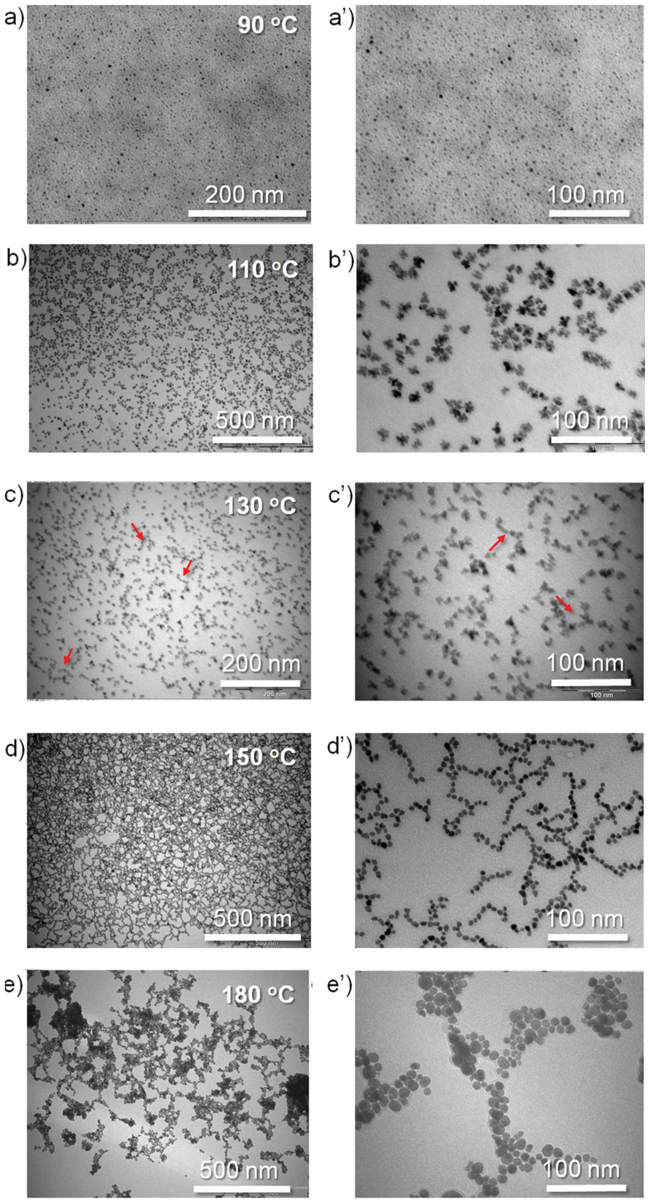

Figure 2. TEM images with different magnifications of Pt nanostructures prepared for 18 h at various reaction temperatures: a,a') 90, b,b') 110, c,c') 130, d,d') 150, and e,e') 180 °C.

kinetic controlled process should be suppressed and the reaction was under thermodynamic control.[33,34] Particles tend to minimize the surface energy through the transformation from the highly faceted multiarmed nanostars to spheres that possess lower specific surface area than nanostars. Further increasing the temperature to 180 °C could lead to damaging the self-assembled structures with bigger spherical nanoparticles (≈12 nm) as building units (Figures 2e,e').

2.3. Magnetism and Electronic Structure of Pt Chain Networks

To determine if the magnetic dipolar interactions induce the Pt nanochain networks, we carried out magnetization measurements for the sample prepared at 160 °C by a SQUID magnetometer (Quantum Design) and the main results were presented in **Figure 3**. The magnetization data of the samples prepared at 110 and 180 °C were also collected for comparison (Figure 3). Figure 3a,b show the M–H curves of the three Pt nanostructures in the applied field range of 0–20 kOe, which indicate that their magnetizations are not saturated up to 20 kOe at 5 K and 300 K. As to the sample prepared at 160 °C, the saturation magnetization should be higher than 0.025 emu g^{-1} at 5 K and 0.013 emu g^{-1} at 300 K inferred from Figure 3a,b, respectively. Figure 3c,d reveal obvious hysteresis loop for the three samples at low fields of the M–H plots, indicating their ferromagnetic behavior even at room temperature. The variations of coercivity H_c and the remanence M_r for the samples prepared at 110, 160, and 180 °C are shown in Figure 3e. It can be found that the magnitudes of H_c and M_r for the sample obtained at 160 °C are much higher than those of the samples obtained at 110 and 180 °C. The above results suggest that the magnetic dipolar interactions may be strong enough to drive the formation of chain-like assemblies at 160 °C. The magnetization property of the three samples was further studied using the standard zero field cooling (ZFC) and field cooling (FC) protocols under an applied magnetic field of 1000 Oe between 5 and 300 K, as shown in Figure 3f. All the samples exhibit a paramagnetic-like Curie-Weiss behavior.[35] However, apparent divergence of the FC and ZFC magnetizations for the samples prepared at 160 (up to 250 K) and 180 °C (up to 125 K) can be observed, which can exclude the para- and diamagnetic contributions to the hysteris loop[36,37] and thus further confirms the ferromagnetism of the as-made Pt nanostructures.

The above samples were also characterized by electron paramagnetic resonance (EPR, microwave frequency: 9.065 GHz) spectroscopy (**Figure 4**), which provides further evidence for the ferromagnetic behavior of these samples. Based on the theory of ferromagnetic resonance,[38] the effective g-factor (g_{eff}) can be determined by $g_{\mathrm{eff}} = h\gamma/\mu_{\mathrm{B}}H_{\mathrm{center}}$, where h, γ, μ_{B}, and H_{center} are Plank constant, frequency of the applied microwave magnetic field, Bohr magnetron, and resonance magnetic field, respectively. Thus, the g_{eff} values for the samples prepared at 110, 160, and 180 °C are ≈2.08, 2.36, and 2.15, respectively, at room temperature. These values are all larger than the free-electron value of 2.0023,[39] indicating the presence of ferromagnetic behavior of these samples.

During the preparation processes, we carefully avoided the use of any magnetic-elements-related objects; however, it is also needed to appraise the possible magnetic impurities quantitatively. To this end, we used the inductively coupled plasma atomic-emission spectroscopy (ICP-AES) technique to determine the magnetic contribution from metal impurities. The results showed that magnetic metals such as Fe, Co, and Ni were all below the detectable limits. Therefore, the experimentally observed ferromagnetism of our samples was their intrinsic properties.

Notwithstanding the existence of ferromagnetism in traditional nonmagnetic materials such as noble metals, semiconductors, and even carbon-based materials[40,41] has been generally accepted, the origin of which is still not fully understood. As to nanoscale Pt, a recent report from Sakamoto et al.

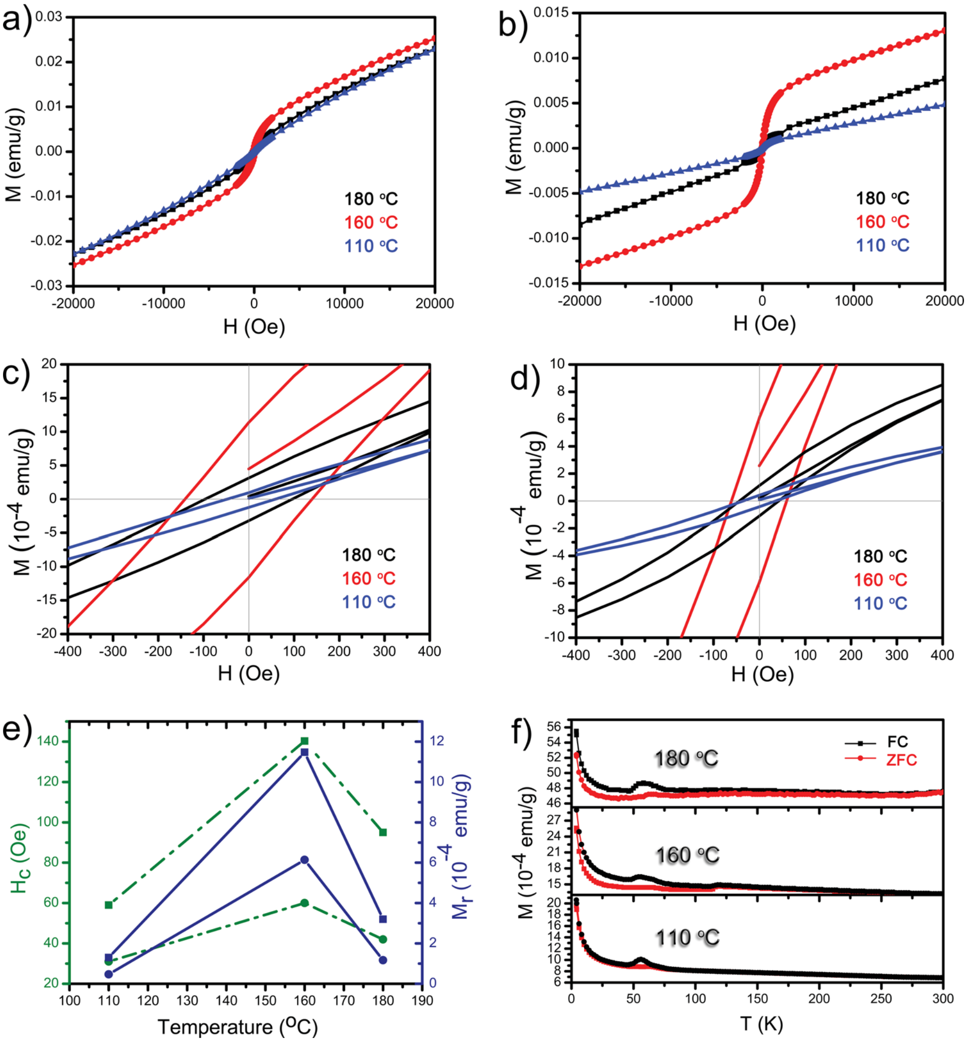

Figure 3. Hysteresis curves recorded at a) 5 K and b) 300 K from the three Pt nanostructures prepared at 110, 160, and 180 °C, respectively. c,d) Corresponding magnified views of the central portion of the loops of (a,b), respectively. e) Coercive field H_c and remanent magnetization M_r extracted from (c,d). (Note: ■, 5 K; •, 300 K) f) Temperature-dependent magnetizations (FC and ZFC) for the three Pt nanostructures measured under applied field of 1000 Oe, respectively.

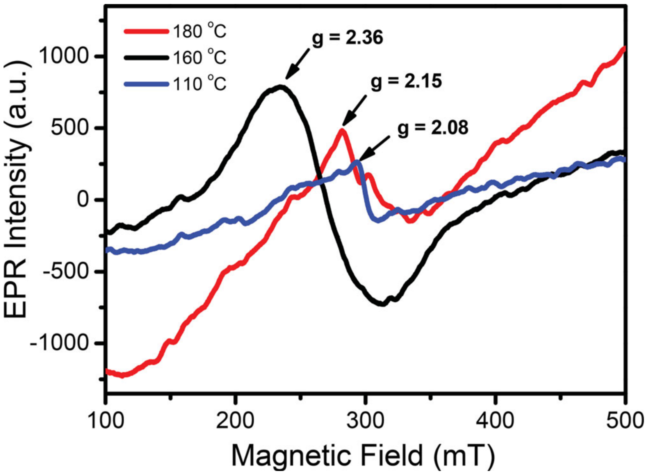

Figure 4. EPR spectra recorded at room temperature for the three Pt nanostructures prepared at 110, 160, and 180 °C, respectively.

summed up several possible mechanisms to interpret its ferromagnetism.[15] It was found that coating molecules are often necessary in that the charge can transfer between the nanoparticle and surrounding coating molecules, leading to the change of electronic structure in Pt.[15] To determine if the ferromagnetism of Pt nanochain networks originated from the interaction of PVP molecules and Pt nanoparticles, we first detected the presence of PVP after synthesis. As shown in **Figure 5**a, the characteristic vibration band of C=O (PVP) located at 1664 cm^{-1} and other vibration bands can be observed for the samples prepared at 110, 160, and 180 °C, respectively, suggesting the existence of PVP in these products. Compared with that of pure PVP, the weak intensity of all vibrations and the absence of several bands presumably are due to the low content of PVP in the Pt nanostructures, which agrees with the HRTEM observation as shown in Figure 1c. For comparison, we also carried out the experiment reacted at 160 °C without PVP as the surfactant. TEM images show that the sample is composed of

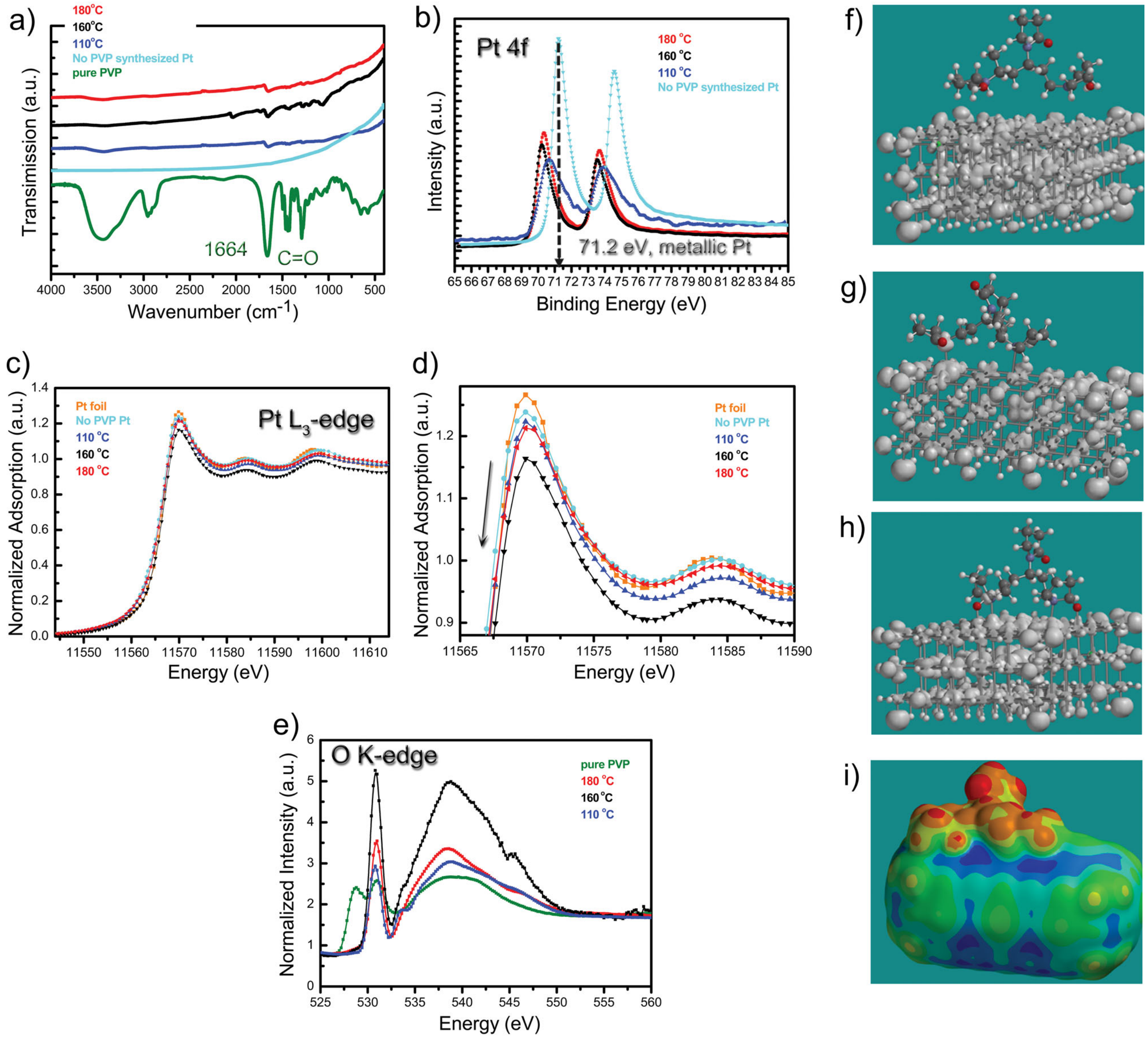

Figure 5. a) FTIR spectra for the Pt nanostructures prepared at different temperatures with PVP, Pt aggregate prepared at 160 °C without PVP, and PVP reference. b) Pt 4f XPS spectra for the Pt nanostructures prepared at different temperatures with PVP and Pt aggregate prepared at 160 °C without PVP. c) Pt L_3-edge XANES spectra for the Pt nanostructures prepared at different temperatures with PVP, Pt aggregate prepared at 160 °C without PVP and Pt foil reference. d) Enlarged region of peaks of Pt L_3-edge XANES white line extracted from (c). e) O K-edge soft XAS spectra for the Pt nanostructures prepared at different temperatures with PVP and PVP reference. f–i) Spin-density maps obtained for three structural models of Pt-PVP NPs with f) intermolecular, g) Pt-N coordination, and h) Pt-N coordination combined with Pt-O covalent bonds between Pt surface and PVP. i) Local ionization potential map for the cluster model in (g). The red/blue color corresponds to the more positive/negative ionization potential and the area of relatively lower/higher electron density.

large aggregates of Pt nanoparticles (Supporting Information, Figure S1). FTIR spectrum of the sample confirms the absence of PVP coating (Figure 5a). The field dependence of magnetization of the sample reveals the paramagnetism of these Pt aggregates at 5 K and 300 K (Supporting Information, Figure S2), acting as their corresponding bulk forms.[18] These results suggest that the coating PVP molecules not only serve as surfactant to stabilize the nanoparticles in solution but also interact with surface atoms of Pt nanoparticles and change their electronic structure, leading to moment stabilization and even the ferromagnetism in Pt nanoparticles.[13,15]

To gain detail insights into the electronic structure change of the PVP-coated Pt nanostructures, X-ray photoelectron spectra (XPS), X-ray absorption near edge structure (XANES), and soft X-ray absorption spectroscopy (XAS) analyses were performed (Figure 5b–d). The electronic states of Pt 4f in Figure 5b show that the binding energies of PVP-coated Pt nanostructures are shifted to lower values compared with no-PVP synthesized Pt (i.e., ≈1.04 eV decrease for 160 °C sample, ≈0.86 eV decrease for 180 °C sample and ≈0.56 eV decrease for 110 °C sample). The change of binding energy for PVP-coated samples is probably due to the electron transfer from PVP to Pt, which is similar to the observation in thin film of Pt/oxide interface.[42] Such electronic structure change in PVP-coated samples was further confirmed by XANES technique. Figure 5c,d show the normalized XANES spectra collected at Pt L_3 edge, from which we can find that intensity of the white line, whose magnitude is a direct measure of occupancy of *d*-band,[43] is in the order Pt foil > no-PVP synthesized Pt > PVP-coated Pt (110 °C) > PVP-coated Pt (180 °C) > PVP-coated Pt (160 °C), with PVP-coated Pt prepared at 160 °C showing the lowest intensity. Here, a lower intensity of the white line is associated with a larger electron transfer from PVP to Pt, which leads to a higher electron density around the Pt atoms and hence a decrease in the 5*d*-band vacancy.[43] The XANES data show good agreement with the XPS results. One question is which atom in the PVP molecule can donate electron to Pt? Using soft XAS technique, we found that O atom in C=O group could make it, which is presented in oxygen K-edge absorption spectra (Figure 5e). Similarly, the band intensity is also linear with the number of holes.[44] It can be found that, after coating the PVP molecules around Pt, the low-energy absorption feature (528–533 eV) increases in intensity, indicating the electron donation from O to Pt. Figure 5e also shows that the most charge transition comes from the 160 °C-synthesized sample and the least one comes from the sample obtained at 110 °C, which agrees well with the XPS (Figure 5b) and the Pt L_3-edge analyses (Figures 5c,d) discussed above.

The appearance of ferromagnetism in nanoscale Pt can be correlated with the interfacial electron density transfer and the bonding strength between PVP and Pt surface. Star-shaped nanoparticles obtained at 110 °C are associated with the weaker bonding primarily due to intermolecular forces. The nanoparticles synthesized at 160 °C and above have stronger binding between PVP and Pt, which can be verified by the progression of FTIR spectra (Figure 5a). We carried out the calculation of spin-density maps of the nanoparticle models by PM3 quantum mechanical algorithm (Figures 5f–i) in order to find the qualitative changes in the magnetic properties which depend on the bonding between Pt and PVP represented by the three cases: I) proximal positioning of PVP to Pt surface (Figure 5f), II) bonding via Pt-N coordination bond (Figure 5g), and III) the bonding via both Pt-N and Pt-O bonds (Figure 5h). These three cases can be related to three temperature regimes during the synthesis, that is, 110 °C, 160 °C, and 180 °C, respectively. Within the limits of structural approximation of the nanoparticles used here, spin-density maps clearly indicate that cases I) and III) show no spill-over of spin-density across the interface in the PVP capping (Figures 5f,h). The case of intermediate bonding via Pt-N coordinating bond demonstrates noticeable transfer of spin-density to the nitrogen atom (Figure 5g). Such spill-over resulted in unusual magnetic properties of the clusters and high sensitivity of the nanoparticle assembly in magnetic fields to the interfacial conditions, which we observed in the experiments. We note that the spin density spill-over also correlates with the general shift of electron density toward Pt based on the local ionization potential map (Figure 5i), which is a consequence of partial charge transfer from PVP to Pt.

2.4. Evolution Process of Pt Chain Networks

To trace the nucleation and growth process of Pt nanochains, a sequence of UV-vis spectra and TEM images recorded at crucial evolution stages (<70 min) were shown in **Figure 6**. For the initial growth solution, a strong peak at 266 nm is from the $PtCl_6^{2-}$,[45] which decays to about 1/2 of its original intensity within 4 min due to the loss of $PtCl_6^{2-}$ (Figure 6a). At 5 min, clear broadening of the peak at 266 nm can be observed, as well as the slight shoulder appeared at ≈247 nm, which is the result of the emergence of Pt(II) intermediate during the reduction process of Pt(IV) to Pt(0).[45] Only one minute later, the peak at 266 nm disappeared and only the peak at 247 nm stayed. We found the solution color changes greatly during the period between 5 and 6 min. Figure 6b shows the optical images recorded at 5′5″, 5′10″, 5′15″, 5′20″, and 6 min, where a quickly darkening color was observed, indicating the reaction evolved very fast during this period. Whereas before 5 min, the solution color was always transparent yellow and no change can be observed. Interestingly, a new peak at 313 nm began to appear at ~ 6.5 min along with the weakening intensity of peak at 247 nm (Figure 6a), which reached the highest intensity at about 26.5 min. This new peak has not been documented previously, which may suggest the formation of a unknown intermediate during the reduction process of Pt(IV) to Pt^0 by ethylene glycol.[45,46] A conclusive answer regarding this needs further investigation. The reduction was completed at 66.5 min, as confirmed by the flat UV-vis spectrum in Figure 6a, and the solution color is nearly black at this stage as shown in Figure 6b.

Figure 6c shows the morphology evolution of Pt nanochains captured at different reaction stages. The burst nucleation triggered by high temperature (160 °C) generates seeds with an average size ≈5.8 nm and the number of the seeds increases rapidly from 5 s to 20 s. At 5 min, some star-like nanoparticles emerged, which continued to appear until consumed all of the Pt seeds (at ≈8 min). These star-like nanostructures resemble the Pt nanostars prepared at 110 °C for 18 h (Figures 2b,b′). HRTEM images of the star-like nanostructures (Supporting Information, Figure S3) revealed that they were single-crystalline, indicating that they were also formed via an overgrowth mechanism rather than through random aggregation of preformed seeds.[31,32] These branched nanostars will evolve into spherical shape from the viewpoint of thermodynamically stability.[33] At this stage, the change in shape and size of nanoparticles is quite limited, which is beneficial to the interaction between the Pt nanoparticles and surrounding PVP molecules. Therefore, the surface electronic structure of Pt was modified by PVP, producing an extrinsic magnetic dipole in Pt nanoparticle. Assembly of Pt nanoparticles will thus emerge by dipolar interactions, as proved by TEM observations in Figure 5 (15–60 min). At 15 min, some Pt nanoparticulate dimers were first formed, which further link together due to the increase in magnetic dipole-dipole interactions and long Pt chains were obtained at 60 min (Figure 6). Eventually, Pt nanoparticles chain networks could be achieved through anisotropic dipolar interactions (Figure 1a), similar

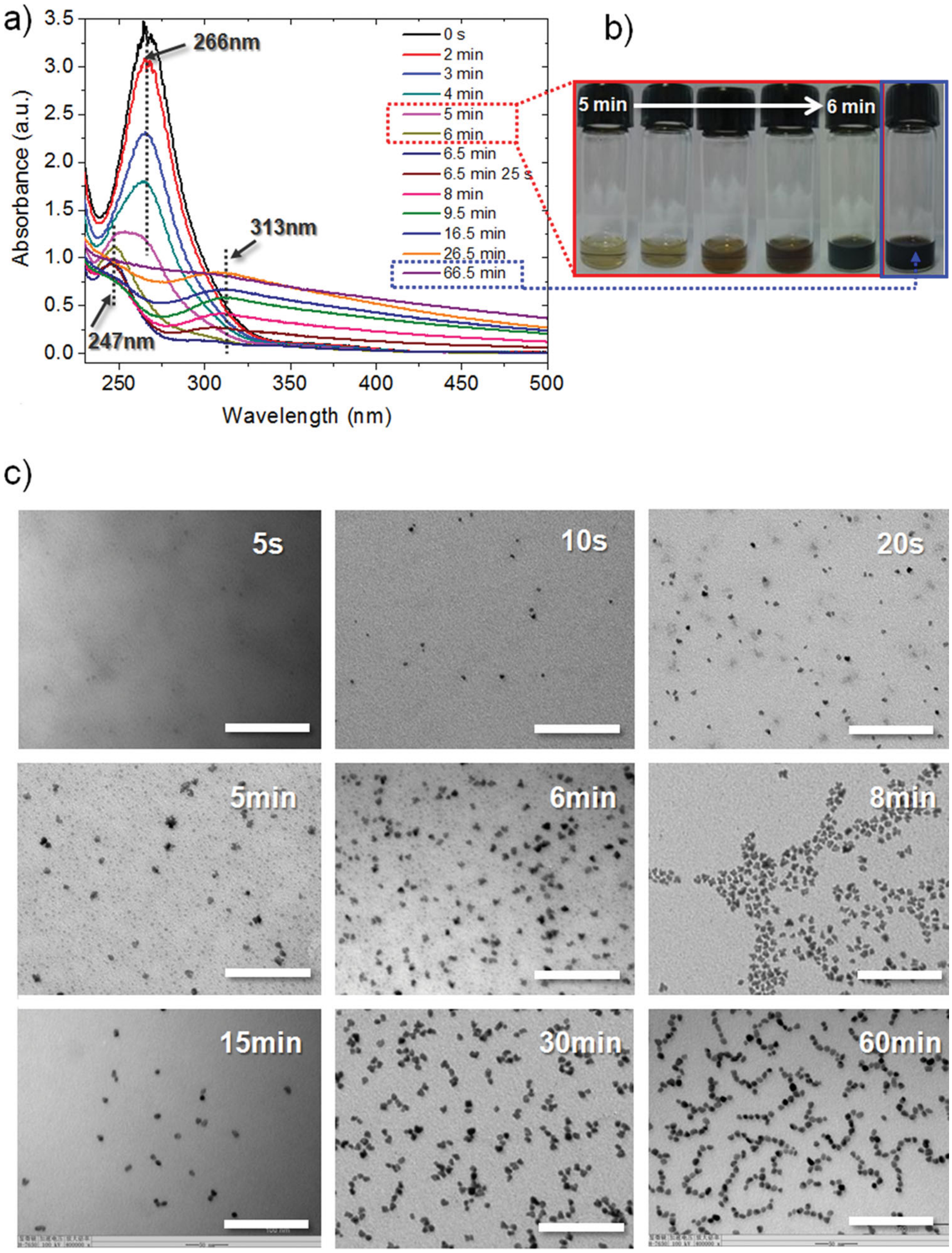

Figure 6. a) UV-vis spectra of reaction solutions taken at different stages of the synthesis. b) Optical images of Pt nanocrystals obtained at the designed times based on the result of UV-vis spectra (a). c) TEM images of Pt nanocrystals made from the samples obtained at different stages of the synthesis. All scale bars are 100 nm.

to dipolar forces induced branched configuration reported by Tlusty and Safran.[47] Of note, the as-synthesized Pt chain networks in solution can be coated by silicon dioxide in aqueous solution (Supporting Information, Figure S4), suggesting that these nanoparticulate self-assemblies were formed directly in the reaction solution by dipolar-dipolar interactions.

3. Conclusions

In summary, we demonstrated that weak ferromagnetic moments can be stabilized in PVP-coated Pt nanocrystals. The electron transfer between PVP molecules and surface Pt atoms can modify the electronic configuration of Pt and induces its ferromagnetism even at room temperature. It has been observed that the in-situ formed magnetic dipole–dipole interactions can drive the organization of Pt nanoparticles into unique chain networks spontaneously in solution. These findings raise a promising opportunity for self-organizing other nonmagnetic nanoscale building blocks into ordered nanostructures by the capped-agent-induced magnetic dipoles, which is highly required for exploring new properties and functionalities of current nanomaterials and thus for their newly emerging technological applications.

4. Experimental Section

Chemicals: All chemicals are of analytical grade and were used as received without further purification.

Synthesis of Pt Chain Networks: The Pt chain networks were prepared by a modified polyol reduction method and a typical procedure was as follows: 4 mL EG was injected into a three-neck flask (25 mL) equipped with a reflux condenser, followed by heating in air at 100 °C for 1 h to boil off trace water. After that, the reaction flask was moved in another oil bath with temperature of 160 °C. Then, 1 mL of freshly prepared PVP solution (0.045 g mL_{EG}^{-1}) and 1 mL H_2PtCl_6 solution (0.033 g mL_{EG}^{-1}) were added dropwise simultaneously to the reaction flask within 1.5 min. The reaction was allowed to continue at 160 °C for another 18 h. The final sample was collected by centrifugation, washed several times by distilled water and ethanol to remove EG and excess PVP, dispersed in ethanol for further use. The temperature and reaction time can be changed to investigate their influence on the synthesis of Pt chain networks (Caution: in order to avoid bringing magnetic metal impurities, all magnetic-metal-related building blocks, such as magnetic stirring bar, were not used during the synthesis).

Synthesis of SiO_2 Coated Pt Chain Networks: A patch of Pt chain networks prepared by the polyol reduction method described above was dispersed into a mixture of 60 mL of isopropanol, 2 mL of deionized water, and 2 mL of ammonium. After vigorous mechanical stirring for 30 min, 2.25 mL tetraethoxysilane solution (TEOS solution, which were obtained by diluting 40 µL of TEOS in 20 mL of deionized water) was injected dropwise with 10 h under mechanical stirring. The mixture was allowed to stir for another 10 h and the final product was centrifugated and redispersed in ethanol.

Characterization: X-Ray powder diffraction (XRD) was carried out on a Rigaku D/max-rA X-ray diffractometer with Cu Ka radiation ($\lambda = 1.54178$ Å). TEM images, HRTEM images, selected-area electron diffraction (SAED), and an energy-disperse X-ray spectrum (EDS) were taken with a JEOJ-2010 transmission electron microscope with an acceleration voltage of 200 kV. The magnetic properties of samples were investigated using a superconducting quantum interface device (SQUID) magnetometer (Quantum Design MPMS XL). Room temperature electron paramagnetic resonance (EPR) spectra were performed on JEOL JES-FA200 EPR spectrometer (300 K, 9064 MHz, X-band). The Fourier transform infrared (FTIR) spectra were measured on a Bruker Vector-22 FT-IR spectrometer at room temperature. The XPS were recorded on an ESCALab MKII X-ray photo-electron spectrometer using Mg Ka radiation exciting source. The XANES measurements were performed in transmission mode at U7C XAFS station in NSRL (National Synchrotron Radiation Laboratory, Hefei, P. R. China). UV-visible absorption spectra were recorded on a Shimadzu DUV-3700 spectrometer. The possible magnetic metal impurities were determined by the inductively coupled plasma atomic-emission spectroscopy (ICP-AES) technique using an Atomscan Advantage (Thermo Jarrell Ash Corporation, U.S.A.) instrument.

PM3 Quantum Mechanical Calculation: The PM3 calculations were performed using SPARTAN 10 quantum mechanical software package from Wavefunctions Co (Irvine, CA, USA) using global convergence settings. The limit for a number of atoms allowable for this package for PM3 algorithm is 500. The initial geometrical optimization was accomplished by Molecular Mechanics subroutine. The clusters calculated were considered to carry a positive charge according to the experimental data.

Supporting Information

Supporting Information is available from the Wiley Online Library or from the author.

Acknowledgements

The authors acknowledge the special funding support from the National Basic Research Program of China (Grant 2010CB934700), the National Natural Science Foundation of China (Grants 91022032, 91227103, 21101051), the Ministry of Science and Technology of China (Grant 2012BAD32B05–4), the Chinese Academy of Sciences (Grant KJZD-EWM01–1), and the Fundamental Research Funds for the Central Universities (2012HGCX0003, WK 2060190021). The authors thank Prof. Nicholas Kotov at the University of Michigan for kind help with PM3 calculations.

Received: July 5, 2013

---

[1] S. Lin, M. Li, E. Dujardin, C. Girard, S. Mann, *Adv. Mater.* **2005**, *17*, 2553.
[2] J. J. Benkoski, S. E. Bowles, B. D. Korth, R. L. Jones, J. F. Douglas, A. Karim, J. Pyun, *J. Am. Chem. Soc.* **2007**, *129*, 6291.
[3] A. P. Philipse, D. Maas, *Langmuir* **2002**, *18*, 9977.
[4] P. Y. Keng, I. Shim, B. D. Korth, J. F. Douglas, J. Pyun, *ACS Nano* **2007**, *1*, 279.
[5] S. L. Tripp, R. E. Dunin-Borkowski, A. Wei, *Angew. Chem. Int. Ed.* **2003**, *42*, 5591.
[6] M. J. Hu, Y. Lu, S. Zhang, S. R. Guo, B. Lin, M. Zhang, S. H. Yu, *J. Am. Chem. Soc.* **2008**, *130*, 11606.
[7] Z. Y. Tang, N. A. Kotov, M. Giersig, *Science* **2002**, *297*, 237.
[8] G. A. DeVries, M. Brunnbauer, Y. Hu, A. M. Jackson, B. Long, B. T. Neltner, O. Uzun, B. H. Wunsch, F. Stellacci, *Science* **2007**, *315*, 358.
[9] S. Mann, *Nat. Mater.* **2009**, *8*, 781.
[10] M. Li, S. Johnson, H. T. Guo, E. Dujardin, S. Mann, *Adv. Funct. Mater.* **2011**, *21*, 851.
[11] X. Liu, M. Bauer, H. Bertagnolli, E. Roduner, J. van Slageren, F. Phillipp, *Phys. Rev. Lett.* **2006**, *97*, 253401.
[12] M. A. Garcia, M. L. Ruiz-Gonzalez, G. F. de la Fuente, P. Crespo, J. M. Gonzalez, J. Llopis, J. M. Gonzalez-Calbet, M. Vallet-Regi, A. Hernando, *Chem. Mater.* **2007**, *19*, 889.
[13] A. Smogunov, A. Dal Corso, A. Delin, R. Weht, E. Tosatti, *Nat. Nanotech.* **2008**, *3*, 22.
[14] H. T. Zhang, J. Ding, G. M. Chow, *Langmuir* **2008**, *24*, 375.
[15] Y. Sakamoto, Y. Oba, H. Maki, M. Suda, Y. Einaga, T. Sato, M. Mizumaki, N. Kawamura, M. Suzuki, *Phys. Rev. B* **2011**, *83*, 104420.
[16] A. Delin, E. Tosatti, R. Weht, *Phys. Rev. Lett.* **2004**, *92*, 057201.
[17] E. Coronado, A. Ribera, J. Garcia-Martinez, N. Linares, L. M. Liz-Marzan, *J. Mater. Chem.* **2008**, *18*, 5682.
[18] X. W. Teng, W. Q. Han, W. Ku, M. Hucker, *Angew. Chem. Int. Ed.* **2008**, *47*, 2055.
[19] Y. Yamamoto, T. Miura, M. Suzuki, N. Kawamura, H. Miyagawa, T. Nakamura, K. Kobayashi, T. Teranishi, H. Hori, *Phys. Rev. Lett.* **2004**, *93*, 116801.
[20] P. Crespo, R. Litran, T. C. Rojas, M. Multigner, J. M. de la Fuente, J. C. Sanchez-Lopez, M. A. Garcia, A. Hernando, S. Penades, A. Fernandez, *Phys. Rev. Lett.* **2004**, *93*, 087204.
[21] X. W. Teng, M. Feygenson, Q. Wang, J. Q. He, W. X. Du, A. I. Frenkel, W. Q. Han, M. Aronson, *Nano Lett.* **2009**, *9*, 3177.
[22] E. C. Stoner, *Philos. Mag.* **1924**, *48*, 719.
[23] I. Carmeli, G. Leitus, R. Naaman, S. Reich, Z. Vager, *J. Chem. Phys.* **2003**, *118*, 10372.
[24] A. Hernando, P. Crespo, M. A. Garcia, E. F. Pinel, J. de la Venta, A. Fernandez, S. Penades, *Phys. Rev. B* **2006**, *74*, 052403.
[25] M. A. Garcia, J. M. Merino, E. F. Pinel, A. Quesada, J. de la Venta, M. L. R. Gonzalez, G. R. Castro, P. Crespo, J. Llopis, J. M. Gonzalez-Calbet, A. Hernando, *Nano Lett.* **2007**, *7*, 1489.
[26] S. Z. Deng, H. M. Fan, M. Wang, M. R. Zheng, J. B. Yi, R. Q. Wu, H. R. Tan, C. H. Sow, J. Ding, Y. P. Feng, K. P. Loh, *Acs Nano* **2010**, *4*, 495.

[27] G. X. Zhu, S. G. Zhang, Z. Xu, J. Ma, X. P. Shen, *J. Am. Chem. Soc.* **2011**, *133*, 15605.
[28] M. S. Seehra, P. Dutta, S. Neeleshwar, Y. Y. Chen, C. L. Chen, S. W. Chou, C. C. Chen, C. L. Dong, C. L. Chang, *Adv. Mater.* **2008**, *20*, 1656.
[29] A. Zakrassov, G. Leitus, S. R. Cohen, R. Naaman, *Adv. Mater.* **2008**, *20*, 2552.
[30] Y. Oba, T. Shinohara, T. Oku, J. I. Suzuki, M. Ohnuma, T. Sato, *J. Phys. Soc. Jpn.* **2009**, *78*, 044711.
[31] M. A. Mahmoud, C. E. Tabor, M. A. El-Sayed, Y. Ding, Z. L. Wang, *J. Am. Chem. Soc.* **2008**, *130*, 4590.
[32] E. Formo, P. H. C. Camargo, B. Lim, M. J. Jiang, Y. N. Xia, *Chem. Phys. Lett.* **2009**, *476*, 56.
[33] X. W. Teng, H. Yang, *Nano Lett.* **2005**, *5*, 885.
[34] J. T. Ren, R. D. Tilley, *J. Am. Chem. Soc.* **2007**, *129*, 3287.
[35] Y. Y. Rao, H. Y. Xu, Y. Liang, S. Hark, *CrystEngComm* **2011**, *13*, 2566.
[36] D. P. Norton, S. J. Pearton, A. F. Hebard, N. Theodoropoulou, L. A. Boatner, R. G. Wilson, *Appl. Phys. Lett.* **2003**, *82*, 239.
[37] Y. J. Kang, D. S. Kim, S. H. Lee, J. Park, J. Chang, J. Y. Moon, G. Lee, J. Yoon, Y. Jo, M. H. Jung, *J. Phys. Chem. C* **2007**, *111*, 14956.
[38] D. Q. Gao, G. J. Yang, J. Zhang, Z. H. Zhu, M. S. Si, D. S. Xue, *Appl. Phys. Lett.* **2011**, *99*, 052502.
[39] J. R. Pilbrow, Transition Ion Electron Paramagnetic Resonance, Clarendon Press, Oxford **1990**.
[40] W. L. Wang, S. Meng, E. Kaxiras, *Nano Lett.* **2008**, *8*, 241.
[41] Y. Wang, Y. Huang, Y. Song, X. Y. Zhang, Y. F. Ma, J. J. Liang, Y. S. Chen, *Nano Lett.* **2009**, *9*, 220.
[42] M. K. Bahl, S. C. Tsai, Y. W. Chung, *Phys. Rev. B* **1980**, *21*, 1344.
[43] B. J. Hwang, S. M. S. Kumar, C. H. Chen, Monalisa, M. Y. Cheng, D. G. Liu, J. F. Lee, *J. Phys. Chem. C* **2007**, *111*, 15267.
[44] F. M. F. Degroot, M. Grioni, J. C. Fuggle, J. Ghijsen, G. A. Sawatzky, H. Petersen, *Phys. Rev. B* **1989**, *40*, 5715.
[45] J. Y. Chen, T. Herricks, M. Geissler, Y. N. Xia, *J. Am. Chem. Soc.* **2004**, *126*, 10854.
[46] Y. N. Xia, Y. J. Xiong, B. Lim, S. E. Skrabalak, *Angew. Chem. Int. Ed.* **2009**, *48*, 60.
[47] T. Tlusty, S. A. Safran, *Science* **2000**, *290*, 1328.